

Determination of the Temperature Field in the Depth of the Body Measurement With a Thermal Imager on the Surface *

Eugenia Homenok, Ivan Ignatiev, Yana F. Ivanova, Dmitriy A. Tarkhov^[0000-0002-9431-8241], Andrey D. Yukhnev and Konstantin Zabello

Peter the Great St. Petersburg Polytechnic University
dtarkhov@gmail.com

Abstract. The use of ultrasound local heating of human body tissues for the treatment of cancer and other diseases is a promising direction in medicine because of its minimally invasive and cheap. The application of this method requires precise control of the localization of thermal effects in a given area. For this purpose, two main methods are used – ultrasonic thermometry and restoration of the thermal field inside the body by measurements on its surface. In this article, we present the results of our theoretical and experimental researches of the s method. The field was reconstructed at depth. This restoration was based on the results of measurements of the thermal imager from the surface of the body during high-intensity focused ultrasound (HIFU) heating. At the same time, we were forced to digitize the graphic data of temperature distribution, which was given by the thermal imager. The results of the restoration were compared with the results of measurements by sensors which was located at different depths. As a result of the comparison, the error was less than 1°C. Subsequently, we took these results as exemplary for testing the accuracy of the ultrasonic thermometry (UST) program. The average time difference between the temperature increase obtained by the UST program and the recovered data is 1.5 °C. We consider that these results are acceptable for further research on biological tissues.

Keywords: ultrasonic thermometry method, focused ultrasound therapy, reconstruction of the temperature field.

1 Introduction

To control the process of thermal effects in the application of focused ultrasound therapy [1] is a usually used method of ultrasonic thermometry [2-6]. To assess the accuracy of the ultrasonic testing method, we conducted an experiment in which HIFU heating of the test object was performed using the thermal imager measured the temperature

* Copyright 2019 for this paper by its authors. Use permitted under Creative Commons License Attribution 4.0 International (CC BY 4.0).

on its surface. According to the results of measurements of the temperature field on the surface of the test object, the field was restored at depth. Results recovery of temperature by depth were taken the sample of the test program UST. In this paper we present the results of the temperature field recovery in the test object. We compare these results with the results of measurements using sensors.

2 Material and methods

The experiment was carried out heating of the tissue-mimicking material (TMM) using the HIFU transducer. The scanning plane of the ultrasonic transducer is perpendicular to the axis of the HIFU transducer. The thermal imager was installed at a height of 15 cm from the surface of the test object and recorded a video with thermal images of the surface of the material during heating and cooling, as well as with the temperature distribution along a 28mm long line passing through the heating center. To control the temperature inside the test object, we installed sensors at depths of 2mm, 4mm, and 6mm and at a distance of 3mm from the center of focus.

To process data from the thermal imager in Matlab, a program was written that allows you to create a graph of the temperature distribution along the line drawn on the device screen. Work with it is as follows: first, the program is loaded with video data obtained by the thermal imager and is divided into frames. Next, the coordinates of the frame area from which the data should be read are set (in this case, the row with the minimum and maximum values of temperatures and the temperature distribution graph were set). Then the characters from the string corresponding to the data type specified in the program are formed into an array. Thus, the output is a table with the maximum and minimum temperature values from each frame of interest to us. At the same time, the original graph is cleared of noise so that the program image consists of a white "background" and a black line. The resulting images contain the temperature and coordinate of each pixel belonging to the graph, that is, an array $A[T, i]$ and $\text{length}(n)$ is formed, where i is the frame number, n is the number of pixels on the x-axis. Since every 10th frame was taken in this experiment, the time interval between frames is 1 s, which means that it is possible to plot the temperature change of a fixed x over time (step – 1 s).

The problem of restoring the temperature field induced by focused ultrasound from measurements on the surface of the test object can be solved in the first approximation in the entire space or in the half-space, neglecting the boundary effects. In this case, the error is minimal when the source is located in the depth of the material and small time intervals.

The first substitution. In this production, the solution is sought throughout the space. This result can be used to restore the solution in the depth of the test object. According to [1], the temperature field in the tissues satisfies the equation

$$\frac{\partial T}{\partial t} = K\Delta T - bT + S(t, \mathbf{x}) \quad (1)$$

Here T - the thermal field, K - the coefficient of thermal diffusivity, b - the coefficient reflecting the heat transfer of blood, $S(t, \mathbf{x})$ - ultrasonic heat source.

According to [1] in cylindrical coordinate system $S(t, \mathbf{x}) = Q(t) \exp[-r^2/\beta_r] \exp[-z^2/\beta_z]$. The result is a solution of the form

$$T(t, r, z) = c \int_0^t Q(\tau) \frac{\exp[-b(t-\tau)] \exp[-r^2/(4K(t-\tau) + \beta_r)] \exp[-z^2/(4K(t-\tau) + \beta_z)]}{\sqrt{4K(t-\tau) + \beta_z(4K(t-\tau) + \beta_r)}} d\tau$$

In the case of a short-term ultrasonic pulse at the initial time, the density of the ultrasonic source is expressed in terms of the Delta function $Q(t) = q\delta(t)$

$$T(t, r, z) = cq \frac{\exp[-bt] \exp[-r^2/(4Kt + \beta_r)] \exp[-z^2/(4Kt + \beta_z)]}{\sqrt{4Kt + \beta_z(4Kt + \beta_r)}}$$

In the first approximation, we can ignore the boundary effects arising from the fact that the problem is solved in half-space, not in space. In this case, the error is minimal when the source is located in the depth of the material and small times.

If a sequence of actions is performed, then, due to the linearity of equation (1), the total thermal field is represented as the sum of the thermal fields of the sources.

S substitution. We will solve equation (1) in half-space. Replacement $T(t, \mathbf{x}) = u(t, \mathbf{x}) \exp[-bt]$ equation (1) is given as

$$\frac{\partial u}{\partial t} = K\Delta u + P(t, \mathbf{x}). \quad (2)$$

Here $P(t, \mathbf{x}) = S(t, \mathbf{x}) \exp[bt]$.

We will solve the problem (2) in the half-space $-\infty \leq x < +\infty, -\infty < y < +\infty, 0 \leq z < +\infty$. Due to the fact that the thermal conductivity of the air is 25-30 times less than that of the test object, we take as a boundary condition $\frac{\partial u}{\partial z} = 0$ by $z = 0$. Then, according to [2]

$$u(t, x, y, z) = \int_0^t \int_{-\infty}^{+\infty} \int_{-\infty}^{+\infty} P(\tau, \xi, \eta, \zeta) G(t - \tau, x, y, z, \xi, \eta, \zeta) d\tau d\xi d\eta d\zeta, \quad (3)$$

$$\text{where } G(t, x, y, z, \xi, \eta, \zeta) = \frac{\exp[-\frac{(z-\zeta)^2}{4Kt}] + \exp[-\frac{(z+\zeta)^2}{4Kt}]}{8(\pi Kt)^{3/2}} \exp[-\frac{(x-\xi)^2 + (y-\eta)^2}{4Kt}].$$

According to [1] $P(t, x, y, z) = \exp[bt]Q(t) \exp[-(x^2 + y^2)/\beta_r] \exp[-(z - z_0)^2/\beta_z]$. Here z_0 - depth of focus of ultrasonic action.

$$\text{Substituting in (3), receive } u(t, x, y, z) = \frac{1}{8(\pi K)^{3/2}} \int_0^t \frac{\exp[b\tau]Q(\tau)}{(t-\tau)^{3/2}} \int_{-\infty}^{+\infty} \exp[-\frac{(x-\xi)^2}{4K(t-\tau)}] \exp[-\xi^2/\beta_r] d\xi \int_{-\infty}^{+\infty} \exp[-\frac{(y-\eta)^2}{4K(t-\tau)}] \exp[-\eta^2/\beta_r] d\eta \int_0^{+\infty} (\exp[-\frac{(z-\zeta)^2}{4K(t-\tau)}] + \exp[-\frac{(z+\zeta)^2}{4K(t-\tau)}]) \exp[-(\zeta - z_0)^2/\beta_z] d\zeta d\tau$$

The last three integrals are calculated analytically.

$$\begin{aligned} \int_{-\infty}^{+\infty} \exp\left[-\frac{(x-\xi)^2}{4K(t-\tau)}\right] \exp\left[-\xi^2/\beta_r\right] d\xi &= 2\sqrt{\frac{\pi\beta_r K(t-\tau)}{\beta_r+4K(t-\tau)}} \exp\left[-\frac{x^2}{\beta_r+4K(t-\tau)}\right] \int_{-\infty}^{+\infty} \exp\left[-\frac{(y-\eta)^2}{4K(t-\tau)}\right] \exp\left[-\eta^2/\beta_r\right] d\eta \\ &= 2\sqrt{\frac{\pi\beta_r K(t-\tau)}{\beta_r+4K(t-\tau)}} \exp\left[-\frac{y^2}{\beta_r+4K(t-\tau)}\right] \int_0^{+\infty} \exp\left[-\frac{(z-\zeta)^2}{4K(t-\tau)}\right] + \\ &\exp\left[-\frac{(z+\zeta)^2}{4K(t-\tau)}\right] \exp\left[-(\zeta-z_0)^2\right] / \\ &\beta_z d\zeta = \sqrt{\frac{\pi K(t-\tau)\beta_z}{\beta_z+4K(t-\tau)}} \left(\exp\left[\frac{-(z-z_0)^2}{\beta_z+4K(t-\tau)}\right] \operatorname{erfc}\left[\frac{z\beta_z+4K(t-\tau)z_0}{2\sqrt{\beta_z K(t-\tau)}\sqrt{\beta_z+4K(t-\tau)}}\right] + \right. \\ &\left. \exp\left[\frac{-(z+z_0)^2}{\beta_z+4K(t-\tau)}\right] \operatorname{erfc}\left[\frac{-z\beta_z+4K(t-\tau)z_0}{2\sqrt{\beta_z K(t-\tau)}\sqrt{\beta_z+4K(t-\tau)}}\right]\right) \end{aligned}$$

Here $\operatorname{erfc}[x] = \frac{2}{\sqrt{\pi}} \int_x^{+\infty} e^{-t^2} dt$ - additional probability integral.

As a result, we get:

$$\begin{aligned} u(t, x, y, z) &= \frac{\beta_r\sqrt{\beta_z}}{2} \int_0^t \frac{\exp[b\tau]Q(\tau)}{(\beta_r+4K(t-\tau))\sqrt{\beta_z+4K(t-\tau)}} \exp\left[-\frac{x^2+y^2}{\beta_r+4K(t-\tau)}\right] \left(\exp\left[\frac{-(z-z_0)^2}{\beta_z+4K(t-\tau)}\right] \operatorname{erfc}\left[\frac{z\beta_z+4K(t-\tau)z_0}{2\sqrt{\beta_z K(t-\tau)}\sqrt{\beta_z+4K(t-\tau)}}\right] + \right. \\ &\left. + \exp\left[\frac{-(z+z_0)^2}{\beta_z+4K(t-\tau)}\right] \operatorname{erfc}\left[\frac{-z\beta_z+4K(t-\tau)z_0}{2\sqrt{\beta_z K(t-\tau)}\sqrt{\beta_z+4K(t-\tau)}}\right]\right) d\tau \end{aligned} \quad (4)$$

The surface temperature distribution that can be measured is as follows

$$\begin{aligned} u(t, x, y, 0) &= \beta_r\sqrt{\beta_z} \int_0^t \frac{\exp[b\tau]Q(\tau)}{(\beta_r+4K(t-\tau))\sqrt{\beta_z+4K(t-\tau)}} \exp\left[-\frac{x^2+y^2}{\beta_r+4K(t-\tau)}\right] \exp\left[\frac{-z_0^2}{\beta_z+4K(t-\tau)}\right] \operatorname{erfc}\left[\frac{2\sqrt{K(t-\tau)}z_0}{\sqrt{\beta_z}\sqrt{\beta_z+4K(t-\tau)}}\right] d\tau \end{aligned} \quad (5)$$

By measurements using the least-squares method, you can restore the coefficients β_r, β_z, K, b and, if necessary, z_0 .

$$\text{If } b = 0, Q(\tau) = \begin{cases} q & \text{if } \tau \leq T \\ 0 & \text{if } \tau > T \end{cases}$$

$$u(t, x, y, 0) = \beta_r\sqrt{\beta_z}q \int_0^{\min(t, T)} \frac{\exp\left[-\frac{x^2+y^2}{\beta_r+4K(t-\tau)}\right] \exp\left[\frac{-z_0^2}{\beta_z+4K(t-\tau)}\right] \operatorname{erfc}\left[\frac{2\sqrt{K(t-\tau)}z_0}{\sqrt{\beta_z}\sqrt{\beta_z+4K(t-\tau)}}\right]}{(\beta_r+4K(t-\tau))\sqrt{\beta_z+4K(t-\tau)}} d\tau$$

Due to the fact that the measurements are carried out at $t > T$, receive

$$u(t, x, y, 0) = \beta_r\sqrt{\beta_z}q \int_{t-T}^t \frac{\exp\left[-\frac{x^2+y^2}{\beta_r+4K\tau}\right] \exp\left[\frac{-z_0^2}{\beta_z+4K\tau}\right] \operatorname{erfc}\left[\frac{2\sqrt{K\tau}z_0}{\sqrt{\beta_z}\sqrt{\beta_z+4K\tau}}\right]}{(\beta_r+4K\tau)\sqrt{\beta_z+4K\tau}} d\tau \quad (6)$$

Introduce the notation $A = \beta_r\sqrt{\beta_z}q$, $B = 4K$, then (6) is slightly simplified

$$u(t, x, y, 0) = A \int_{t-T}^t \frac{\exp\left[-\frac{x^2+y^2}{\beta_r+B\tau}\right] \exp\left[\frac{-z_0^2}{\beta_z+B\tau}\right] \operatorname{erfc}\left[\frac{\sqrt{B\tau}z_0}{\sqrt{\beta_z}\sqrt{\beta_z+B\tau}}\right]}{(\beta_r+B\tau)\sqrt{\beta_z+B\tau}} d\tau \quad (7)$$

Let the measurements take place over a period of time $\Delta t = h$, $t = nh$, $T = Nh$, $\tau = ih$. To estimate the integral, we use the formula of averages

$$u(nh, x, y, 0) = Ah \sum_{i=1}^N \frac{\exp[-\frac{x^2+y^2}{\beta_r+B\tau_{n+i}}] \exp[-\frac{z_0^2}{\beta_z+B\tau_{n+i}}] \operatorname{erfc}[\frac{\sqrt{B\tau_{n+i}}z_0}{\sqrt{\beta_z}\sqrt{\beta_z+B\tau_{n+i}}}]}{(\beta_r+B\tau_{n+i})\sqrt{\beta_z+B\tau_{n+i}}}, \quad (8)$$

where $\tau_k = (k - N - 0.5)h$

Parameters β_r, β_z, A, B are found by the least-squares method by minimizing the expression

$$\sum_{n,j,k} (u(nh, x_j, y_k, 0) - u_{n,j_k})^2 \quad (9)$$

where u_{n,j_k} - the measured temperature at the corresponding point.

3 Calculation

Due to the fact that the measurements of the thermal field sensors were carried out in the test object at a shallow depth, the s substitution of the problem was used. Figure 1 shows the change in the temperature increment in time on the surface of the test object in the heating center according to the thermal imager and reduced by the formula (6).

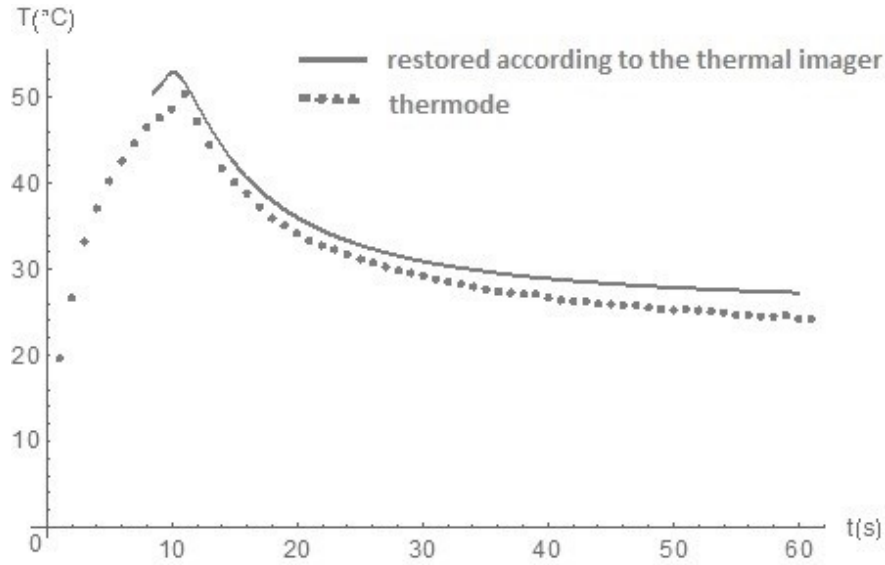


Fig. 1. Comparison of the measured thermal imager and the reduced temperature in the heating center

The graph shows that the difference between the temperature measured by the thermal imager and the temperature restored by the formula (6) in the heating center by the above method is about a degree.

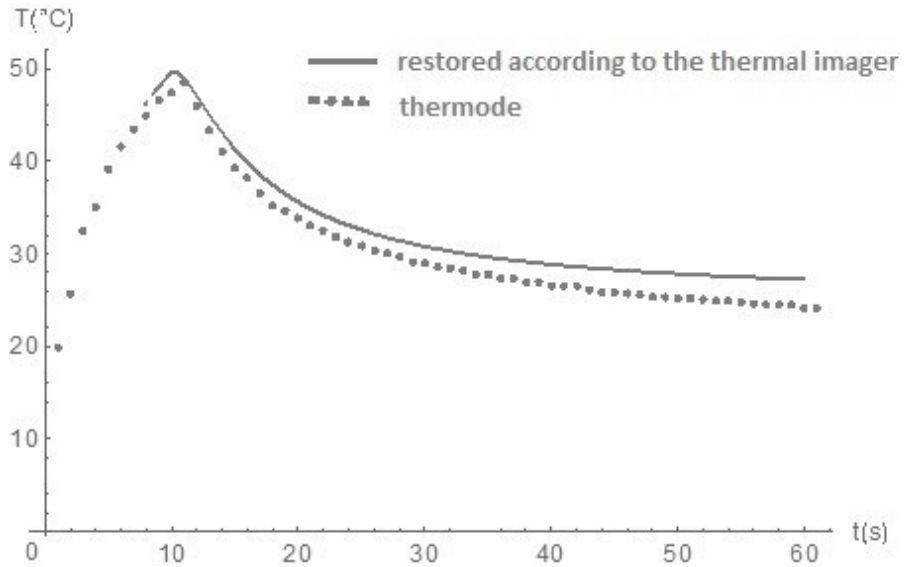


Fig. 2. Comparison of the measured thermal imager and the restored temperature at a distance of 1.2 mm from the center

It can be seen from figure 2 that the difference between the temperature measured by the thermal imager and the temperature restored by the formula (6) at a distance of 1.2 mm from the heating center by the above method is about two degrees.

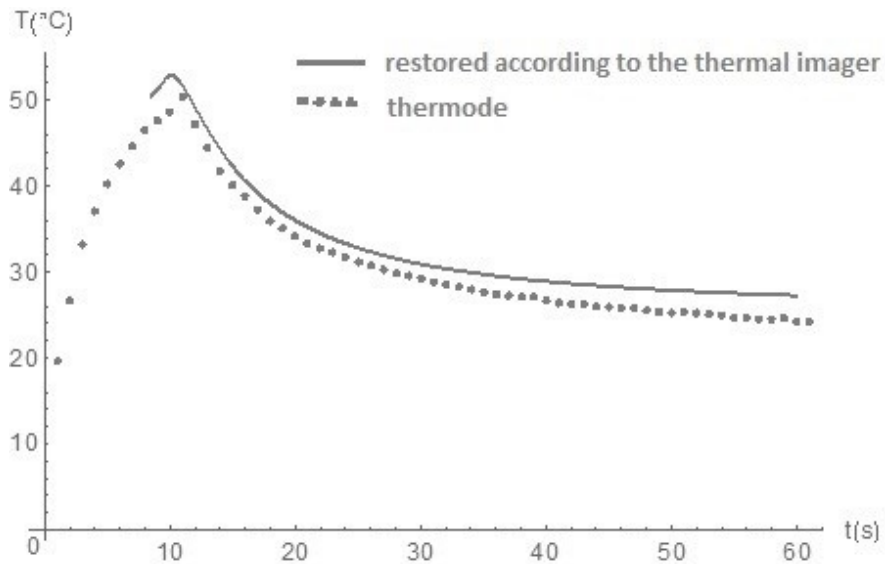


Fig. 3. Comparison of the measured thermal imager and the restored temperature at a distance of 2.4 mm from the center

It can be seen from figure 3 that the difference between the temperature measured by the thermal imager and the temperature restored by the formula (6) at a distance of 2.4 mm from the heating center by the above method is about three degrees.

Figures 1-3 show that the proposed model of temperature distribution during HIFU heating of the test object reflects the experimental data quite well. The error increase while rising the distance from the heating center is caused by the neglect of heat transfer into the air.

On fig. 4-6 the change of temperature increment in time at a depth of 2 mm, 4 mm and 6 mm from the surface of the test object and a distance of 3mm from the heating center, restored according to the thermal imager according to the formula (6) and measured by a temperature sensor is given.

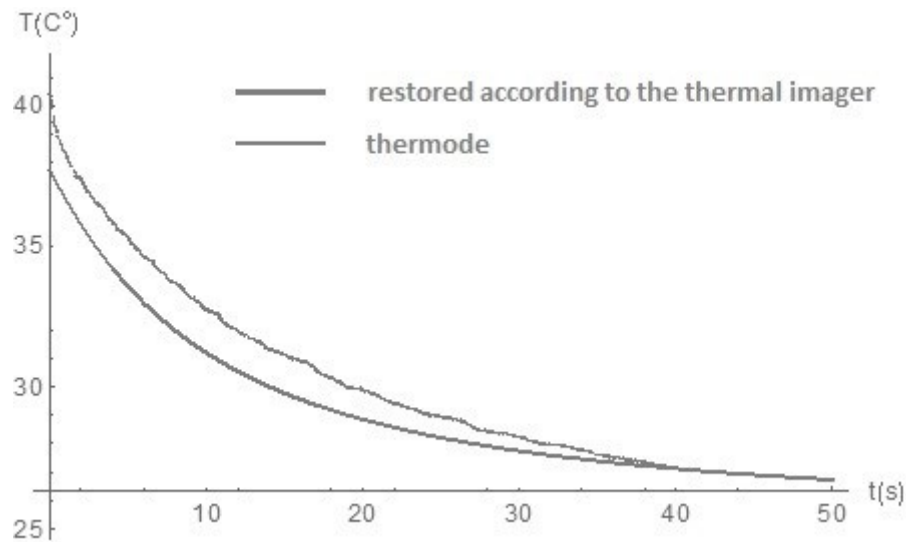


Fig. 4. Comparison of the measured and reduced temperature at a depth of 2mm from the surface of the TMM and a distance of 3m from the heating center

It can be seen from the graph that the difference between the measured temperature and the thermal imager restored according to the above method is about a degree.

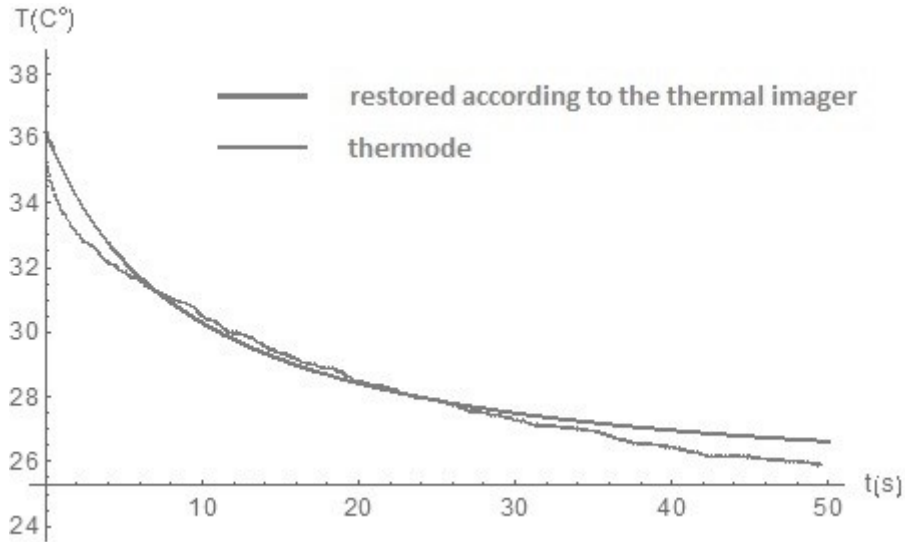


Fig. 5. Comparison of measured and restored temperature at a depth of 4 mm from the TMM surface and a distance of 3 mm from the heating center

It can be seen from the figure that the difference between the measured temperature and the temperature which was restored by the above method at a depth of 4 mm from the surface is about 0.5 degrees.

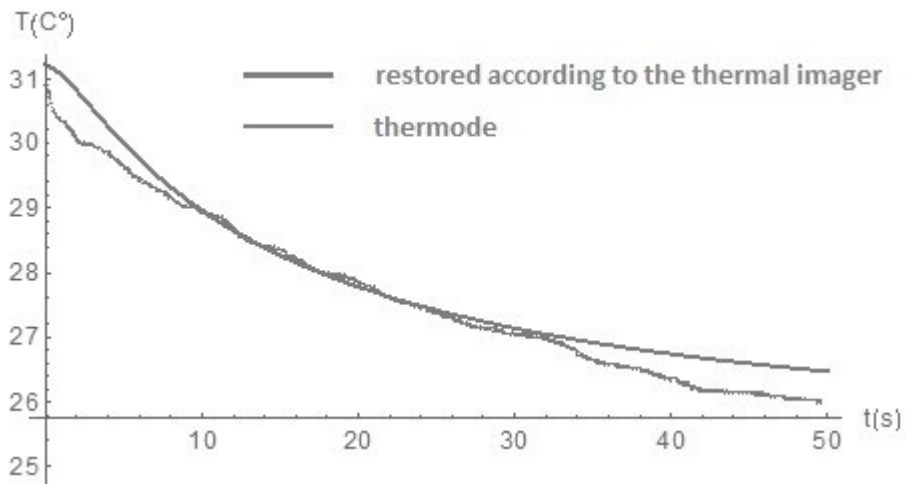


Fig. 6. Comparison of the measured and reduced temperature at a depth of 6m from the TMM surface and a distance of 3m from the heating center

It can be seen from the graph that the difference between the measured temperature and the thermal imager restored according to the above method is about a half degree.

4 Results and Discussion

Based on the above results, we can conclude that the described method of restoring the temperature field by the results of measurement on the surface can be considered quite accurate. It should be especially noted that the error in determining the temperature field in the depth of the test object (the measurements of which were not used in the construction of the model) is no more than an error in the approximation of the temperature field on the surface (which was used in the construction of the model). In addition, from a computational point of view, it is more efficient than the UST method. Besides the UST method, we tested the neural network approach for the described problem [8-16]. Due to the fact that it is necessary to use sufficiently large neural networks and labor-intensive training procedures to obtain acceptable accuracy, the specified neural network approach is not suitable for monitoring the temperature field during HIFU-heating as the real-time operation is required.

5 Conclusions

The results of the studies that we have given above, allow us to regard the described method as quite accurate and effective. We recommend using that method in ultrasound therapy in the treatment of cancer, malignant tumors, and other diseases.

Acknowledgment.

The study was carried out in the framework of Project No. RFMEFI57818X0263 supported by the Education and Science Ministry of the Russian Federation for 2018-2019.

References

1. Khokhlova V.A., Crum L.A., ter Haar G., Aubry J.-F. (Eds.) High Intensity Focused Ultrasound Therapy. Berlin: Springer 500 p. (2017)
2. Zhou Y. Noninvasive Thermometry in High-Intensity Focused Ultrasound Ablation. *Ultrasound Quarterly*. 33 (4). 253-260. (2017)
3. Hsiao Y.-S., Deng C.X. Calibration and Evaluation of Ultrasound Thermography using Infrared Imaging. *Ultrasound Med Biol*. 42(2). 503-517. (2016)
4. Ebbini E.S., Simon C., Liu D., Real-Time Ultrasound Thermography and Thermometry *IEEE Signal Process. Mag.*, 35, 166-174 (2018)
5. Berkovich A.E., Smirnov E.M., Yukhnev A.D., Gataulin Y.A., Sinitsyna D.E., Tarkhov D.A. Development of ultrasound thermometry technique using tissue-mimicking phantom. *IOP Conf. Series: Journal of Physics: Conf. Series* 1044 12023 P.7 (2018). DOI: 10.1088/1742-6596/1044/1/012023
6. Anand A., Kaczkowski P. Noninvasive measurement of local thermal diffusivity using backscatter ultrasound and focused ultrasound heating. *Ultrasound in Med. & Biol*
7. A. D. Polyanin. *Handbook of Linear Partial Differential Equations for Engineers and Scientists*. Boca Raton-London: Chapman & Hall/CRC Press, 2002

8. Antonov V., Tarkhov D., Vasilyev A. Unified approach to constructing the neural network models of real objects. Part 1 // *Mathematical Models and Methods in Applied Sciences*, 2018 Volume 41, Issue 18 Pages: 9244-9251
9. Lagaris I.E., Likas A., Fotiadis D.I. Artificial Neural Networks for Solving Ordinary and Partial Differential Equations// *IEEE Transactions on Neural Networks*. – 1998. – Vol.9, No. 5. – pp. 987-1000. DOI: 10.1109/72.712178
10. Dissanayake M.W.M.G., Phan-Thien N. Neural-network-based approximations for solving partial differential equations// *Communications in Numerical Methods in Engineering*. – March 1994. – Volume 10, Issue 3. – pp. 195-201.
11. Fasshauer G. E. Solving differential equations with radial basis functions: multilevel methods and smoothing// *Adv. in Comp. Math.* – 1999. – 11. – pp. 139-159
12. Fornberg B., Larsson E. A Numerical Study of some Radial Basis Function based Solution Methods for Elliptic PDEs// *Computers and Mathematics with Applications*. – 2003. – 46. – pp. 891-902
13. Galperin E., Pan Z., Zheng Q. Application of global optimization to implicit solution of Partial Differential Equations// *Computers & Mathematics with Applications*. – Pergamon Press Ltd. – 1993. – Vol. 25, No. 10/11. – pp. 119-124.
14. Galperin E., Zheng Q. Solution and control of PDE via global optimization methods// *Computers & Mathematics with Applications*. – Pergamon Press Ltd. – 1993. – Vol. 25, No. 10/11. – pp. 103-118
15. Sharan M., Kansa E.J., Gupta S. Application of the Multiquadric method to the numerical solution of elliptic partial differential equations// *Applied Mathematics and Computation*. – 1997. – 84. – pp. 275-302
16. T.V. Lazovskaya, D.A. Tarkhov and A.N. Vasilyev Parametric Neural Network Modeling in Engineering, *Recent Patents on Engineering*, Volume 11, Number 1, 2017, pp. 10-15